VOL. 17, NO. 2, JANUARY 2022 ISSN 1819-6608
ARPN Journal of Engineering and Applied Sciences

www.arpnjournals.com

TENSILE, MACROGRAPHIC AND FRACTOGRAPHIC EXAMINATIONS OF FRICTION STIR SPOT WELDED LAP JOINTS OF AA5083-H116

Omolayo M. Ikumapayi[1], Esther T. Akinlabi[2, 3], Ayuba S. Osinubi[3], Abegunde O. Olayinka[4], Olawale S. Fatoba[3] and Stephen A. Akinlabi[5]
[1]Department of Mechanical and Mechatronics Engineering, Afe Babalola University, Ado Ekiti, Nigeria
[2]Pan African University for Life and Earth Sciences Institute (PAULESI), Ibadan, Nigeria
[3]Department of Mechanical Engineering Science, University of Johannesburg, Johannesburg, South Africa
[4]Material Science, Energy and Nanoengineering, Mohammed VI Polytechnic University, Morocco
[5]Department of Mechanical Engineering, Butterworth Campus, Walter Sisulu University, South Africa
E-Mail:ikumapayi.omolayo@gmail.com

ABSTRACT

Failure of welded materials in lap configuration due to poor adhesion bond or shear strength can lead to catastrophic damage to life and properties. Due to exponential demands for joined or welded components in lap configuration mode, it has become imperative to investigate and understand how a solid state joining process parameter can affect joint efficiency. Thus, this research study focuses on the effect of rotational speed and dwell time on the mechanical properties and the failure mode. Friction stir spot welding was used for the welding process. Three rotational speeds of 600, 900 and 1200 rpm and three dwell times of 5, 10 and 15 secs were used for the welding process. From the mechanical testing of the tensile shear strength, it was noticed that the magnitude of the tensile shear strength (TSS), tensile yield strength (TYS) and the fracture force (F.F.) depend on the choice of the rotational speed and dwell time. The maximum shear strength was found at the mid-rotational speed of 900 rpm. Ductile failure mode was noticed for all the samples during the fractography observations. Visual observation of the keyhole defects revealed that the diameter and depth of the keyhole were influenced by the process parameters, which also impacts the weld integrity and quality.

Keywords: aluminium alloy, fracture force, friction stir spot welding, tensile shear strength, tensile yield strength.

1. INTRODUCTION

There is currently high demand on the materials joining involving lap configuration of different thicknesses and sizes in most industrial sectors such as marine, manufacturing, automobile, aeronautic, railways etc., in which friction stir spot welding is actively involved. In the past, industries have been engaging in riveting and bolting for such lap joining and which are not effective and, as such, not reliable because of stress concentration at the joints. Another technology engaged for lap joining has been fusion welding. In this technique, the infusion of enormous heat altered the properties of the materials being welded and is not suitable for thin materials. Friction stir spot welding (FSSW) has a significant advantage compared to fusion or arc welding process problems such as solid solidification, cracking, porosity is eliminated during the FSSW process because of its solid-state nature. Both FSSW and friction stir welding (FSW) processes display the presence of deformation and microstructure differences in their weld zone, including the nugget zone (N.Z.), heat affected zone (HAZ) and the thermomechanical affected zone (TMAZ).

Friction stir spot welding (FSSW) was developed at the discovery of an extension of friction stir welding (FSW) for joining aluminium alloys and other metallic alloys [1]. Friction stir spot welding (FSSW) is a technology that took its variance from friction stir welding (FSW) that produces its welded joints by plunging a fabricated non-consumable rotating tool composing a shoulder as well as a probe into two-lap plates in which it dwells for some seconds and then retracting the rotating tool leaving a keyhole at the centre of the spot [2, 3]. Since the FSSW is a solid-state welding process, no coolant is needed because the welding takes place within few seconds, known as the dwell time. Also, power consumption is less in the process than resistant-spot welding, which consumed a high volume of electricity. The ability to weld materials below their melting point makes solid-state welding processes preferred over other welding processes in the manufacturing industries. Solid-state welding has several advantages over other welding processes. Some of these advantages include reduced width of intermetallic compounds, lower heat input, low residual stresses, reduced thermal distortion, good weld appearance, refined microstructure, improved mechanical properties, enhanced corrosion properties and reduced weld defects [4, 5]. Proper selection of welding parameters in solid-state welding is essential for optimum joint performance [5]. FSSW has no traverse movement after plunging a rotating non-consumable tool into the workpiece [6]. There are two primary rotating non-consumable tools components used in FSSW, which are pin and shoulder. The pin is designed to disrupt the faying surface of the workpiece and transport the materials around, which produce deformation and friction heat in the workpiece. In contrast, the tool shoulder produces most of the frictional heat to the surface and subsurface region of the workpiece.

The penetration of the tool shoulder is proportional to the total thickness of the lap materials and the pin length. The shoulder diameter and the pin probe play distinct roles during FSSW because the shoulder diameter of the tool first meets the surface of the upper plate just after the pin penetration enters the second plate

beneath. It will be noticed that both the probe and the shoulder tool will generate intense heat and pressure, leading to plastic deformation of the materials under investigation. Subsequently, a welded joint is achieved. The two-lap plates become an entity [7]. Aside from the role of non-consumable welding tools, several other factors influenced the welds' integrity, such as the dwell time, which plays a cogent role during FSSW, tool plunge depth, and the tool rotational speed, which play major roles during FSSW [1]. The role of travel or traverse speed during FSSW was never noticed since there was no movement of the welding tools during FSSW. It was only dwelled at a spot and then retracted. The careful selection of the parameters determines the strength and the surface integrity of the welded joints. Inappropriate choice of welding parameters may lead to voids, hook, onion rings, and bonding ligaments during FSSW [8].

Aluminium alloys with several advantages (high strength and low-density) compete with composite materials for weight reduction and emission reduction in many structural components [9]. Depending on the possibility of precipitation hardening, aluminium alloys are classified into heat treatable and non-heat-treatable aluminium alloys. On the other hand, based on the significant alloying element for wrought aluminium, aluminium alloys are classified into series as 1xxx series (greater than 99 % aluminium), 2xxx series (copper as the alloying element), 3xxx series (manganese as the alloying element), 4xxx series (silicon as the alloying element), 5xxx series (magnesium as the alloying element), 6xxx series (magnesium and silicon as the alloying elements), 7xxx series (zinc as the alloying element), 8xxx series (other elements as the alloying elements) and 9xxx series (unused series) [2, 10, 11].

Aluminium alloy series 5xxx has been used extensively in modern life based on the following characteristics such as low density, high strength, high ductility, excellent formability, and high corrosion resistance. The weldability of aluminium alloy varies depending on the chemical composition of the alloy used. The 5XXX series aluminium alloy most especially (5083) alloy which we employed in this research contain the following chemical properties: Zr (0.037 %), Ti (0.025 %), Si (0.195 %), Fe (0.18 %), Cu (0.09 %), Mn (0.662 %), Mg (4.745 %), Cr (0.111 %), Zn (0.042 %) and the rest contain the pure Aluminum which has good corrosion. Also, one of the disadvantages of aluminium alloy (5083) is it has low strength in its welded joint using conventional (fusion) welding methods [1, 8, 12-15].

Integration of aluminium alloy and other materials due to the capability of achieving significant weight reduction for structural applications in various industries has attracted exciting research. However, due to incompatibility in the thermal and chemical properties of aluminium alloys and other metals/alloys, achieving quality joint integrity remains a challenge. Although other welding processes, especially solid-state welding processes, have been used to achieve dissimilar weld joints of aluminium alloy and other materials, they are not without some challenges, such as high equipment cost and need for accurate fixture assembly, to mention but a few.

Tamasgavabari *et al*. [12] investigated the effect of vibration on the mechanical and microstructural properties of metal inert gas welded AA5083-H321 aluminium alloy. A vibration ranging from 400 N to 1000 N was introduced during the welding process to examine their effect. Compared to the samples without vibration, there was about 3 % improvement in the tensile strength. Also, the percentage elongation increased by 6 %, 9 % and 16.5 % when 400 N, 750 N and 1000 N vibration were applied, respectively. There was also a significant reduction in the mean grain size of the vibrated samples. However, the hardness values of the samples were not affected by the vibration.

Zhu *et al*. [13] examined the effect of the fluid flow model in the molten pool on the incomplete fusion and porosity defects of inert metal gas welded AA5083 aluminium alloy. It was observed that three weld bead geometries (convex or flat, or concave) could be achieved by varying the welding current. Insufficient heat input, upward fluid flow, and gas film presence between the molten pool and the sidewall were identified as the causes of incomplete fusion. At the same time, the occurrence of porosity was attributed to the downward fluid flow of the molten pool near the sidewall.

Su *et al*. [16] successfully welded aluminium alloy 5052 to galvanized mild steel by the metal inert gas welding process. The study investigated the effect of different modes of current on the microstructural and mechanical properties. Three intermetallic compounds of iron and aluminium (Fe_2Al_5, $FeAl_3$ and Fe_3Al) were formed in the microstructure. An average ultimate tensile strength of about 201 MPa and 115 MPa was observed when the joints were welded by double pulsed alternate-current and direct-current pulsed metal inert gas welding processes. The fracture occurred in the aluminium base metal when the alternate-current mode was used. In the sample welded with direct current mode, fracture occurred between the Fe_2Al_5 and the steel interface. The better tensile strength observed with alternate-current mode was attributed to the reduced heat input, which led to the formation of thinner intermetallic compounds.

Qiu *et al*. [17] joined aluminium alloy 5052 and mild steel by resistance spot welding process. There was the formation of $FeAl_3$ within the vicinity of the weld and reaction layer, which comprised Fe_2Al_5 and $FeAl_3$ on the mild steel side and aluminium side, respectively. Zhang *et al*. [18] obtained the dissimilar joint of aluminium alloy 5052 and pure copper. It was observed that there was a critical heat input beyond which the microstructure of the weld zone changed, and the failure mode of the joint transformed from ductile pull-out mode to cleavage mode. Mastanaiah *et al.* [19] reported dissimilar electron beam welded porosity free joint of aluminium alloys AA2219 and AA5083. The mathematical model developed in the study revealed the dependence of the mechanical properties on the geometry of the weld bead and softening of the heat-affected zone of the AA5083. The softening was brought about by the reduction of the dislocation

density due to the high heat input. The tensile breaking load of the dissimilar joint obtained by the electron beam welding process was slightly higher than the AA5083 base metal but lower than the AA2219 base metal. However, in terms of percentage elongation, the reverse was the case. AA5083 displayed higher elongation than the joint, while the elongation of the AA2219 base metal was slightly lower than that of the joint.

It is known that 5000 series are primarily used in the marine industry and other industries such as aerospace, automotive, aviation, and nuclear power generation. On this note, it is imperative to fabricate this series of aluminium that is difficult to weld using conventional means. Friction stir spot welding has been identified as one of the best techniques to join this type of material that is used in corrosive environments, especially when lap welding will be involved in which riveting, bolting, and resistance spot welding has been used in the past, which added to the weight and materials cost. Hence, the integrities of the fabricated joints are examined via visual observation, mechanical testing and fractography analysis to establish their suitability for use in the designated environment.

2. METHODOLOGY

2.1 Friction Stir Spot Welding Process

Aluminium AA5083 alloy sheets of 600 mm X 300 mm X 4 mm dimensions, which were later cut into the required dimensions (200 mm X 30 mm X 4 mm) with a smooth surface finish, was used for this research work. The friction stir spot welding processes were performed on an A 2T linear numerically control friction stir welding machine manufactured by ETA technology PVT Ltd, Bangalore, with W.O No: WS0040773 located at Indian Institute of Technology (IIT), Kharagpur, West Bengal, India. Table-1 summarizes the different welding process parameters used to produce the welds. A tilt angle of 2° and plunge depth of 0.2 mm were kept constant and used for all the different welding parameters presented in Table-1. FSSW begins with a clean workpiece firmly clamped to the backing plate already provided on the FSW machine platform. The FSSW programme is computed by inputting parameters, after which the tool assembly moves to the welding start position. After the spindle starts to rotate, the tool is plunged into the workpiece dwelling for some seconds to achieve a sufficiently plasticized state. The tool is then moved along the desired direction with a specified combination of rotational and translation speeds, but in this case, the tool did not move in a traverse direction since the welding is spot welding and there was no traverse movement. The tool is retracted from the workpiece after reaching the weld length as defined in the welding programme. The FSW tool used is a cylindrical AISI H13 steel tool hardened to 52 HRC. An essential tool geometry was used with a probe length of 5.mm, and probe diameter of 6 mm. The tool shoulder diameter is three times the pin diameter (18 mm) and concave geometry to exert pressure on the workpiece during welding. A backing plate made of mild steel was positioned between the bed of the FSW platform and the workpiece. The choice of the backing plate is for proper dissipation of heat during the welding process. A supporting sheet of the same thickness was placed underneath the upper plate to help align and stabilize the sheets to be joined during welding.

Table-1. Process parameters used for the friction stir spot welding.

Process Parameters	Sample notation								
	S1	**S2**	**S3**	**S4**	**S5**	**S6**	**S7**	**S8**	**S9**
Rotational speed (rpm)	600	900	1200	600	900	1200	600	900	1200
Dwell time (sec)	5	5	5	10	10	10	15	15	15
Tilt angle (Degree)	2								
Plunge depth (mm)	0.2								

2.2 Tensile Testing

Tensile shear was conducted on the welded samples using Xforce P-type Zwick/Roell Z250 Tensile tester following ASTM B557M-10 and ASTM E8M-13 standard test methods [20, 21]. The tensile shear tests were carried out using a load cell capacity of 100 kN at a strain rate of 1 mm/min. Three measurements were performed for each process parameter. The schematic illustration of the tensile shear conducted is presented in Figure-1a, while the Zwick/Roell Z250 tensile equipment used is illustrated in Figure-1b.

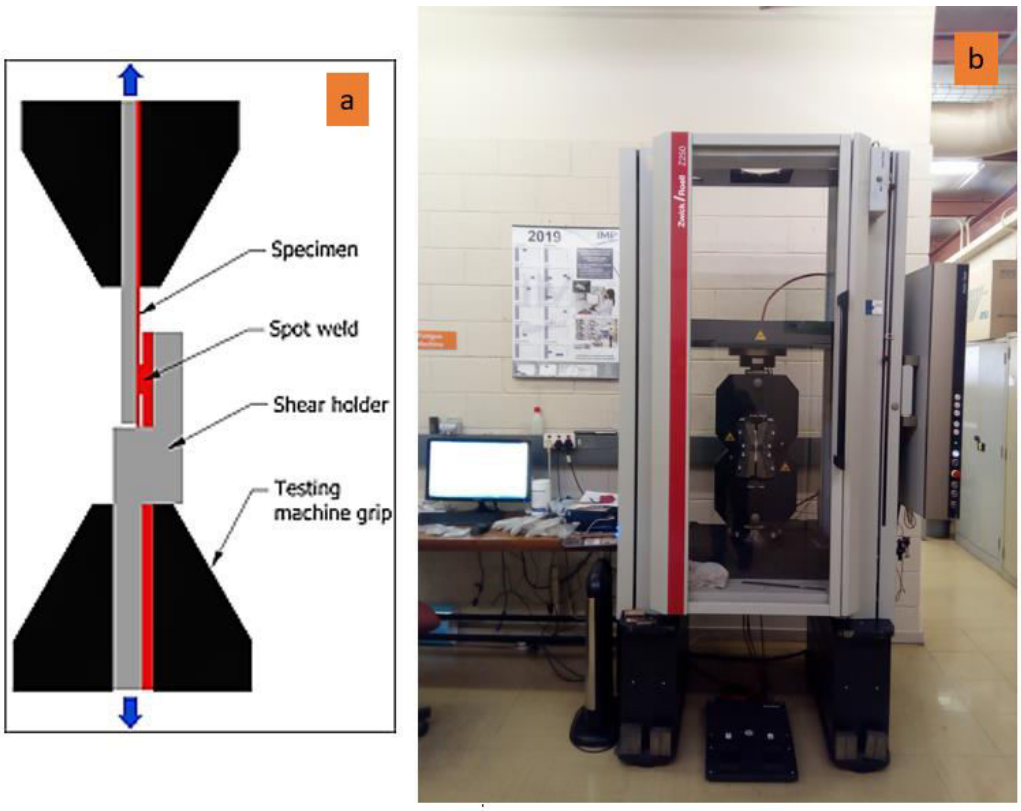

Figure-1. The schematic illustration of the tensile shear (b) Universal testing machine (Zwick/Roell Z250).

2.3 Fractography and Keyhole Analysis

In this study, TESCAN Scanning Electron Microscope (SEM) equipped with Oxford Instrument which was incorporated with Energy-dispersive X-ray spectroscopy (EDXS) - TESCAN model, type VEGA 3 LMH was used to capture the fracture surfaces. The fractured surface was cleaned with acetone to remove surface impurities before the SEM analysis. Olympus optical microscope was used to acquire the images for the keyhole in the welded samples. Before acquiring the fractured surface images, the surface was properly cleaned with acetone and ethanol to remove surface contaminants.

3. RESULTS AND DISCUSSIONS

This section presented the results from the macroscopic visual observation of the keyholes in the welded samples. This also explains the results from the tensile test to determine the shear strength of the spot-welded and fractographical examination taken with the scanning electron microscope. The comparison analysis was adopted for the process parameters used, and the optimum process parameter was established.

3.1 Visual Appearance of Friction Stir Spot Welds Samples

The physical observation of the friction stir spot welded samples were conducted to examine the surface appearance and surface integrity of the welded plates after each processing, as depicted in Figure-2. This is to ensure that there is adequate plunge depth on the lap joint being welded and prevent defects from occurring, such as incomplete penetration, tunnel, cracks, hooks, onion rings, and bonding ligament [22]. The surfaces of all the samples were characterized by the presence of smooth semi-circular streaks at the contact surface between the shoulder and the plate without any irregularities such as flashes or discontinuity. These smooth streaks and the absence of defects show that the tool rotational speeds and dwell times selected for the welds are good processing parameters for the material [23]. A macroscopic examination of the friction stir spot welded samples are examined in the next section to reveal more information about possible defects in the material and flow in the material during each welding.

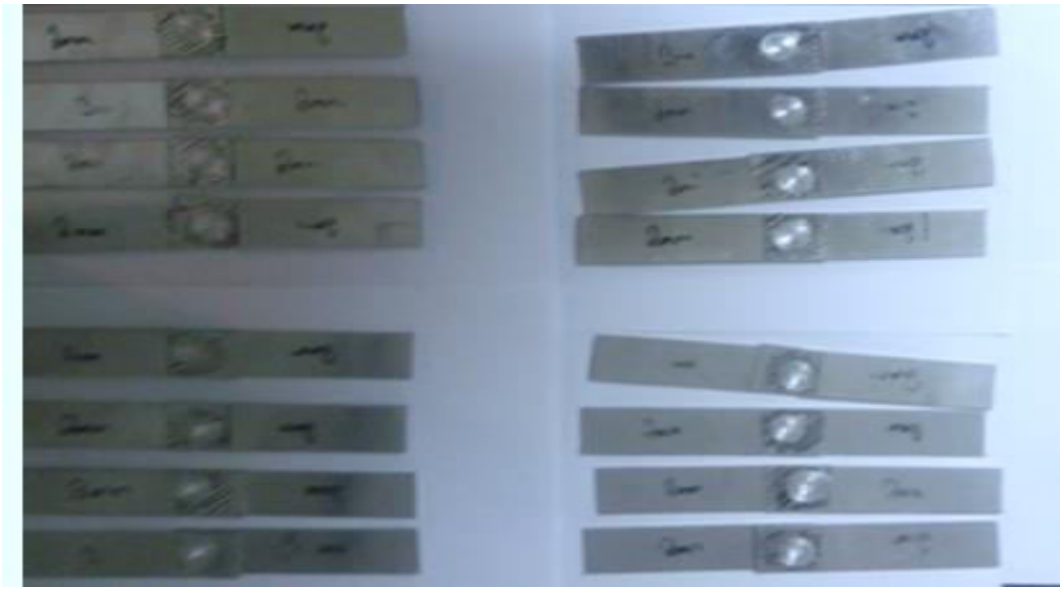

Figure-2. Physical appearances of friction stir spot welds samples.

3.2 Macrostructural Examination

Prior to the determination of the selection of the suitable process parameters, during the trial process to determine the best welding parameters for the spot welding of aluminium alloy AA5083-H116, some welded samples were carried out with some selected parameters. They are welding speeds at 400 rpm, 1800 rpm and 2000 rpm. It was noticed that the defects occurred because the welding speed is too low, and some selected speeds are too high. The resulting lap welded joints were full of defects, as revealed by macroscopic examination in Figure-3. The defects occurred because of wrong or inappropriate selection of welding parameters such as dwell time, plunge depth, tool rotational speed, and tilt angle. Another factor that may contribute to these defects may be improper clamping of the plates to the machine bed, or perhaps there is no damping tool to absorb vibration during the welding process. This can transfer to the workpiece and cause a significant defect [24, 25]. After several trials on the process parameters, a suitable range of welding parameters were obtained. These are the parameters that gave the defect-free zone after welding, and the surface integrity of the welded samples was not compromised. These parameters are then used for the spot-welding process.

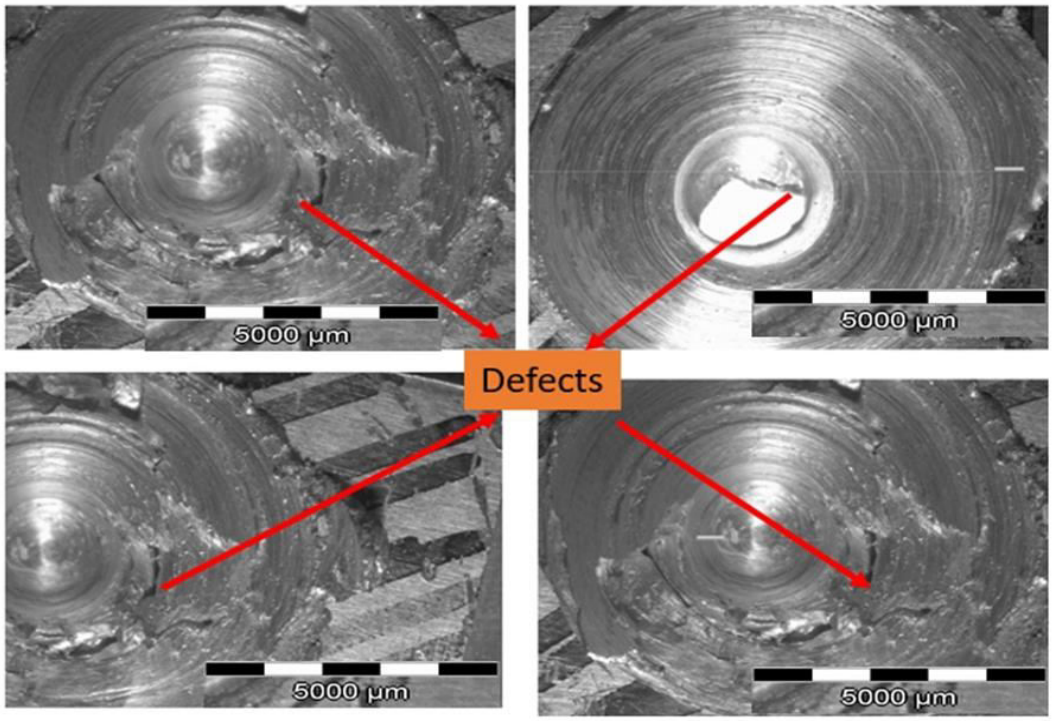

Figure-3. Defects in the spot welds during optimization of welding parameters.

After suitable welding parameters have been achieved, the macrographic examination results revealed that no typical physical defect of FSSW like wormhole, cracks, and void was observed on the surface. There were good appearances with continuous surface defect-free, which implies that the process parameters used were optimized. In the absence of surface asperities, further characterizations were done on all the samples. From this revelation, it can be deduced that tool rotational speed, dwell time, tilt angle, and plunge depth have lots of roles to play in friction stir spot welding to achieve defect-free and best surface integrity. In this macrographic examination, the morphology of the welded surfaces was taken at the magnification of 5000 µm. This spot welding was done on the 4 mm thickness plates of aluminium alloy 5083-H116, which was welded by a cylindrical, tapered pin tool made of AISI H13 steel tool. As mentioned earlier, the dwell time used was 5, 10 and 15 seconds, while the tool rotational speed used was 600, 900, and 1200 rpm with constant parameters of a tilt angle of 2 degrees and plunge depth of 0.2 mm. Figure-4 represents the macrograph of the defect-free friction stir spot welded samples. The welding was done at a rotational speed of 600 rpm leading to S1, S4 and S7 corresponding to dwell times of 5, 10 and 15 seconds, respectively. While at the rotational speed of 900 rpm, it is depicted as S2, S5 and S8, which corresponds to 10, 20- and 30-seconds dwell time, respectively. Whereas, at 1200 rpm tool rotational speed, we have S3, S6, and S9, which corresponds to 5, 10 and 15 seconds, respectively. After the trials process and suitable parameters have been obtained, the welded samples gave defect-free zones.

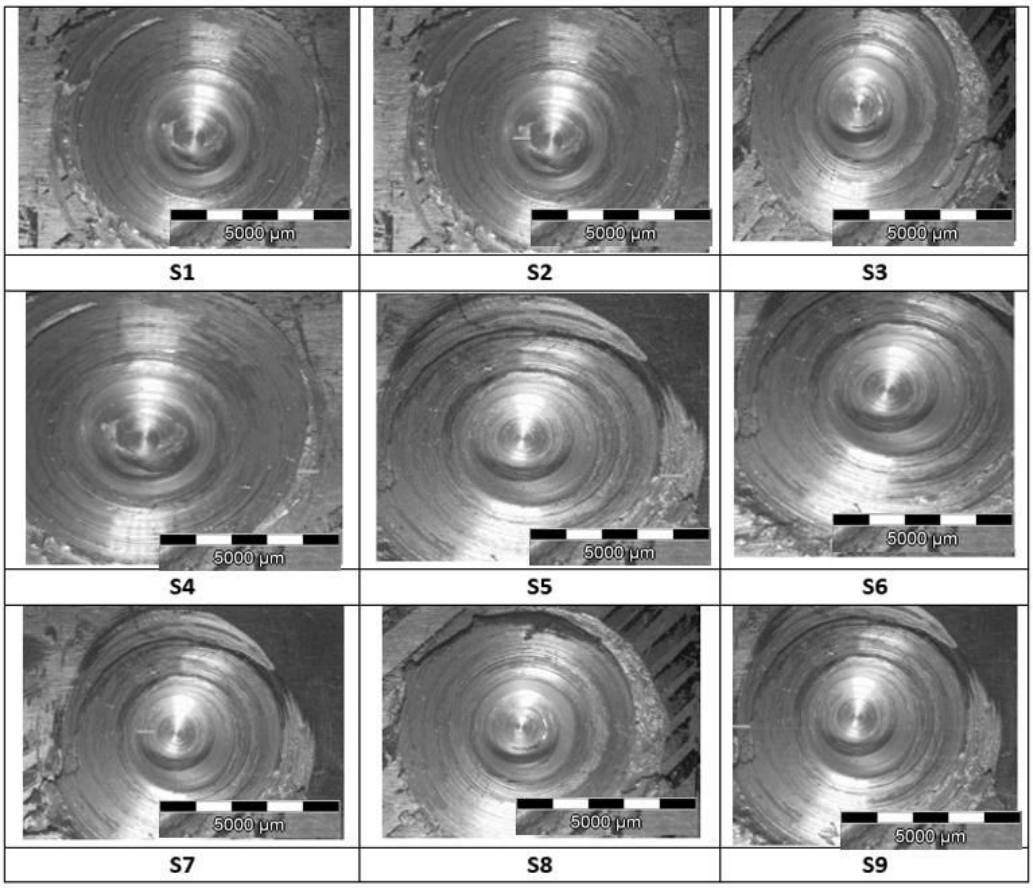

Figure-4. Macrographs of the FSSW showing the top view of the weld zone.

3.3 Tensile Shear Strength of AA5083-H116 FSSW Lap Joints

To determine the strength of the FSSW samples, there are usually two types of tests that can confirm the integrity of the welded strength. It can either be tensile shear or cross tension tests. In this present study, the tensile shear test was adopted to ascertain strength integrity. Figure-5 depicts tensile shear specimen showing stress mechanism due to shear stress such that Φd represents diameter, τx represents shear stress, t is for thickness, while F is for tension-shear, i.e. fracture force. Tensile behaviour, especially tensile shear strength during FSW and FSSW, has been attributed to influential factors by several authors, which are primarily plunge depth dwell time, tilt angle, and tool rotational speed [26-33]. Meanwhile, some researchers argued that only tool rotational speed played a key role while dwell time plays no significant role [8]. The results of the tensile experiment conducted are displayed in Table-2. In this study, the tensile shear test was performed on the lap joint of the spot-welded samples using Xforce P-type

Zwick/Roell Z250 tensile testing machine according to ASTM standard as shown in Figure-5.

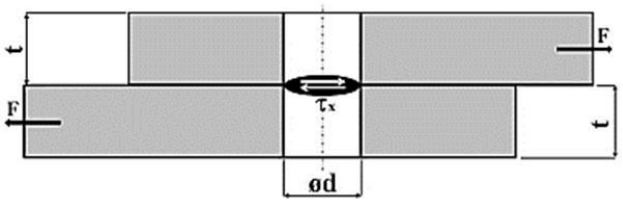

Figure-5. Joints lap configuration of FSSW specimen for tensile shear test.

Table-2 shows the results of the tensile test conducted for samples S 1 - S 9. It was noted that three different rotational speed was used at an interval of 300 from 600 to 1200 rpm. A constant plunge depth of 0.2 mm was used throughout the welding process while the tilt angle was set to 2 degrees. The welding times varying from 5 to 15 seconds with a step of 5 seconds. During the tensile testing, some parameters were measured and recorded, which are fracture force (F.F.), tensile shear strength (TSS), tensile yield strength (TYS) as well as elongation. The percentage of FSSW samples elongation was assessed by measuring the final length of the failed specimens to determine sample ductility. The percentage of elongation is set out in equation (1) according to the report from [32, 33].

$$\%El = \left[\frac{L_f - L_o}{L_o}\right] X\ 100 \quad (1)$$

The values of the tensile test presented are average values of three measurements, and the standard deviation was also calculated to quantify the variance over all nine samples in the observed values. Figure-6 provides a graphical representation of the tensile shear stress against elongation for all the welded samples. Figure-7 also shows detailed tensile behaviour, providing a comparative representation of the friction stir spot welded material graph for all spot welds around the nine samples.

Table-2. Tensile strength results.

Experimental code	Plunge depth (mm)	Dwell time (s)	Rotational Speed (rpm)	Fracture force (kN)	Tensile Shear Strength, TSS (MPa)	Tensile Yield Strength, TYS (MPa)	Elongation (%)
S1	0.2	5	600	10.66	296.34	277.00	7.88
S2	0.2	5	900	12.65	351.62	274.70	11.18
S3	0.2	5	1200	11.20	311.42	271.70	9.52
S4	0.2	10	600	10.42	289.68	278.69	7.52
S5	0.2	10	900	13.02	361.70	266.86	12.61
S6	0.2	10	1200	11.40	317.70	270.70	9.62
S7	0.2	15	600	11.05	307.10	273.90	9.68
S8	0.2	15	900	13.17	365.84	273.93	16.67
S9	0.2	15	1200	11.40	318.86	307.79	9.32

From the results in Table-2, it was observed that the standard deviations of the values in the tensile shear strength (TSS) and tensile yield strength (TYS) are in the range of 7-14. The B.M. from the manufacturer datasheet had yield strength of ~288 MPa, a UTS of ~317 MPa, and a ductility of 16% at break. It was clear that all the FSSW samples show a reduction in tensile and yield strength compared to B.M. samples in some cases except at S 9, which is 1200 rpm and 15 seconds welding time where TYS was 307 MPa with an increase of 19 MPa amounting to 6.5 % improvement. There were reductions in the elongation percentage varying from 7.52 to 12.61 % from the different welding times used. At the same time, the S8 sample exhibited a little bit higher elongation percentage compared to B.M., which is 16.67 % as against 16 % B.M. This shows that the welding parameters used in this work do not significantly impact the ductility of the material.

It can be inferred from Table-2 that fracture forces range from 10.42 to 13.17 kN, tensile shear strength, TSS ranges from 289.68 MPa to 365.84 MPa, the elongation also ranges from 7.52 to 16.67 while tensile yield strength, TYS ranges from 266.86 MPa to 307.79 MPa. It can also be deduced from Table-4.4 that at 600 rpm, the TSS values are 296.34 MPa, 289.68 MPa, and 307.10 MPa at 5 sec, 10 sec, and 15 sec dwell time, respectively. From this result, 15 secs dwell time seems to produce the highest TSS value at this welding parameter of 600 rpm. As depicted in Figure-4.8, the elongation varies at this 600 rpm, from 7.88 %, 7.52 %, and 9.68 %, and this shows that 15 seconds welding time produced the highest elongation of 9.68 %, which is still lower than the 16 % of the base material. It was revealed the highest fracture forces, F.F. was recorded at 900 rpm at 5 sec, 10 sec as well as 15 seconds which correspond to 12.65, 13.02, and 13.17 kN, respectively and this produced shear strength, TSS of 351.62 MPa, 361.70 MPa as well as 365.84 MPa respectively. At this point, their tensile yield strength (TYS) generated 274.70 MPa, 266.86 MPa, and

273.93 MPa with corresponding elongations of 11.18 %, 12.61 %, and 16.67 %, and this can be shown graphically in Figure-6. One can infer from this result that dwells time of 15 seconds produced the highest TYS of 273.93 MPa and the highest Elongation of 16.67 %, which also produced the highest fracture force of 13,17 kN with the highest TSS of 365.84 MPa. In the case of 1200 rpm, the TSS recorded are 311.42 MPa, 317.70 MPa, and 318.86 MPa, which corresponds to 5 sec, 10 sec, and 15 secs welding time. It can be observed that there was a close range in the TSS values at 1200 rpm with 1 to 7 MPa variation, which still falls within the acceptable standard. At this 1200 rpm, the elongation produced was 9.52 %, 9.62 %, and 9.32 %, showing some closed ranges, as depicted in Figure-6.

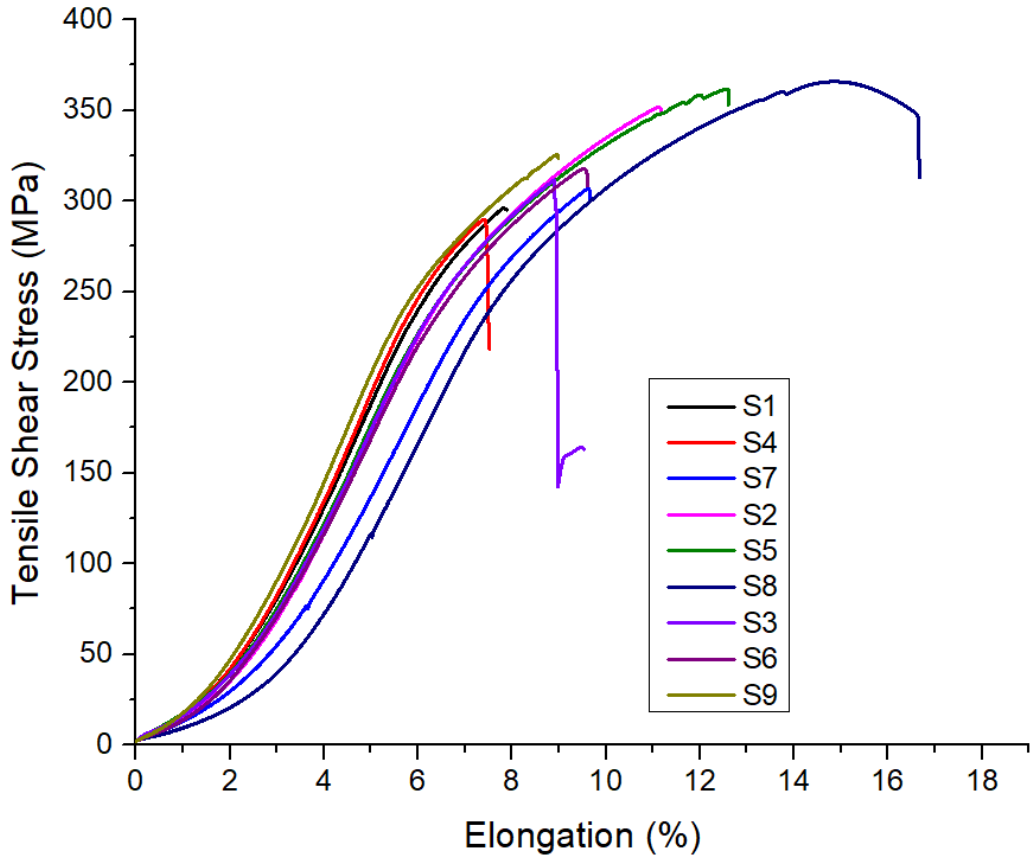

Figure-6. Comparison of the tensile shear stress against elongation for all the spot welds.

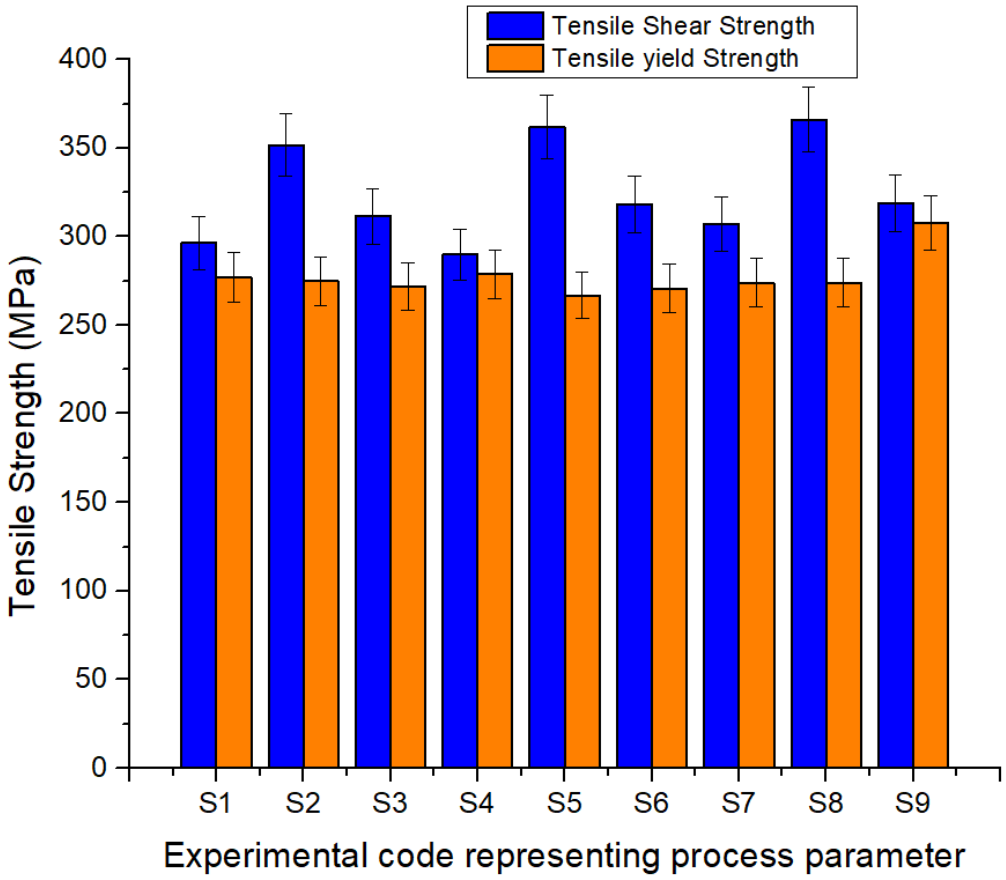

Figure-7. Graphical representation of the tensile properties of the spot-welded samples at 5 % error bar.

Figure-7 shows a comparative assessment of the tensile shear strength results for all the spot-welded samples at a different rotational speed of 600 to 1200 rpm with varying dwell times of 5 seconds to 15 seconds. Each of the tested samples is represented by different coding colours. The graph in Figure-7 shows that all the samples spot-welded at 900 rpm produced the highest elongation and highest tensile shear strength. Similar trends were also noticed when comparing the TSS and TYS of the produced samples in Figure-7. Samples S2, S5 and S8 produced the highest TSS among others, and from this, we can affirm that the best welding parameters are achieved at 900 rpm since this produced the highest strength for the fabricated spot-welds. The TSS produced at 900 rpm is all higher than the UTS of the B.M., which is 351.62 MPa, 361.70 MPa, and 365.84 MPa as against 317 MPa of the B.M. and this may be attributed to the efficacy of the effective and homogenous stirring of the zones at those parameters. It can also be seen from the graph that samples S3 produced TSS values a bit lower than B.M., which was 311.42 MPa, while samples S6 and S9 had almost the same value of TSS with UTS of the B.M., which is 317.70 MPa and 318.86 MPa respectively and this occurred at 1200 rpm. It will be noted that the least values of the TSS were recorded at 600 rpm. The values of TSS at 600 rpm are 296.34 MPa, 289.68 MPa, and 307.10 MPa. This slight reduction may be because of improper stirring at the welded zone or because of inclusion in the welded zone, which may affect the integrity of the welds produced [34, 35]. Unlike the TSS, all the values produced for TYS are higher than the yield strength of the base metal (B.M.), which is ~228 MPa for AA5083. As seen in Figure-7, the TYS produced ranges from 266 MPa to 307.79 MPa, leading to an increment of about 16.67 % to 34.65 % TYS.

3.4 Fractographic Examination of the Fractured Tensile Samples

A fracture is the fragmentation of an object or material into two or more parts during stressful activity. Scientists, therefore, need to elucidate the principles for fractures. There are two categories of fractures. The first is a brittle fracture that occurs without notice under the circumstances and may cause significant material harm. A brittle fracture happens without warning unexpectedly and catastrophically. It is a product of the spontaneous and quick spreading of cracks. However, the presence of plastic deformation gives notice that failure is inevitable for ductile fracture, which allows for preventive steps. The study of fracture mechanics can facilitate a comprehensive understanding of how fracture arises in materials. The second category is a ductile fracture. The ductile fracture is a kind of rupture accompanied by severe plastic deformation or "necking", generally just before an actual fracture occurs. The term "ductile rupture" incorporates a wide range of ductile material faults. In such situations, materials break apart rather than crack. Some parametric

attributes affect the fracture mechanism of Aluminum alloy during fabrication, such as materials used as well as reinforcement volumes and if the particle sizes are in nano-, micro- as well as macrometric form, reinforcement particle distribution, more so the matrix and interface property - this may include precipitation influence, as well as interface contact bonding strength. The material failure during fabrication can be attributed to three distinct sources, namely improper stirring, a matrix breakdown, and interfacial decohesion in the second phase [36, 37]. The fracture aspect in the tensile test is the location of strain at which the material exists separately. At this stage, the pressure reaches its full value, and the material eventually cracks, although, at this point, the resulting stress might be smaller than the ultimate force. Ductile materials have less fracture resistance than the ultimate tensile resistance (UTS), whereas fracture resistance is equal to UTS in brittle materials. If a ductile material exceeds its maximum tensile strength in a load-controlled case, it will continue to bend, with no additional charge application, until it splits.

Nevertheless, if the load is controlled by displacement, the material deformation may relieve the load, thus preventing rupture. Some unique features can be differentiated among the stress-strain graphs of different material groups. Useful knowledge on the basic role of intrinsic microstructural effects on strength and ductility properties is provided by a thorough and detailed inspection of the broken surfaces with tensile. At the microscopic scale, a thorough examination of fracture surfaces revealed minute differences in overall fracture morphology and inherent fracture features. Figure-8 represents the fractography of the fracture surfaces from a tensile test. It was revealed that all the fracture surfaces show ductility behaviours through the morphological examination of the rupture surfaces. The fractography shows in samples S1 - S9 indicated that most of the broken surfaces are occupied by the transgranular caused by dimples, which is consistent with the exceptional interfacial bonding caused by the friction stir spot welding [38]. All the fracture surfaces had large networks of dimples that revealed a two-fold increase in the morphology of the fracture surface that further tells the nature of fracture division. A pattern of large dimples on the morphology of the fracture surfaces improved interface bonding excellently by the interaction of the welding tools and the lap metal matrix during FSSW, and this enhancing mechanical property. This ductility pattern of the fracture surfaces was due to considerable and significant plastic deformation, which is caused by the enormous load [39].

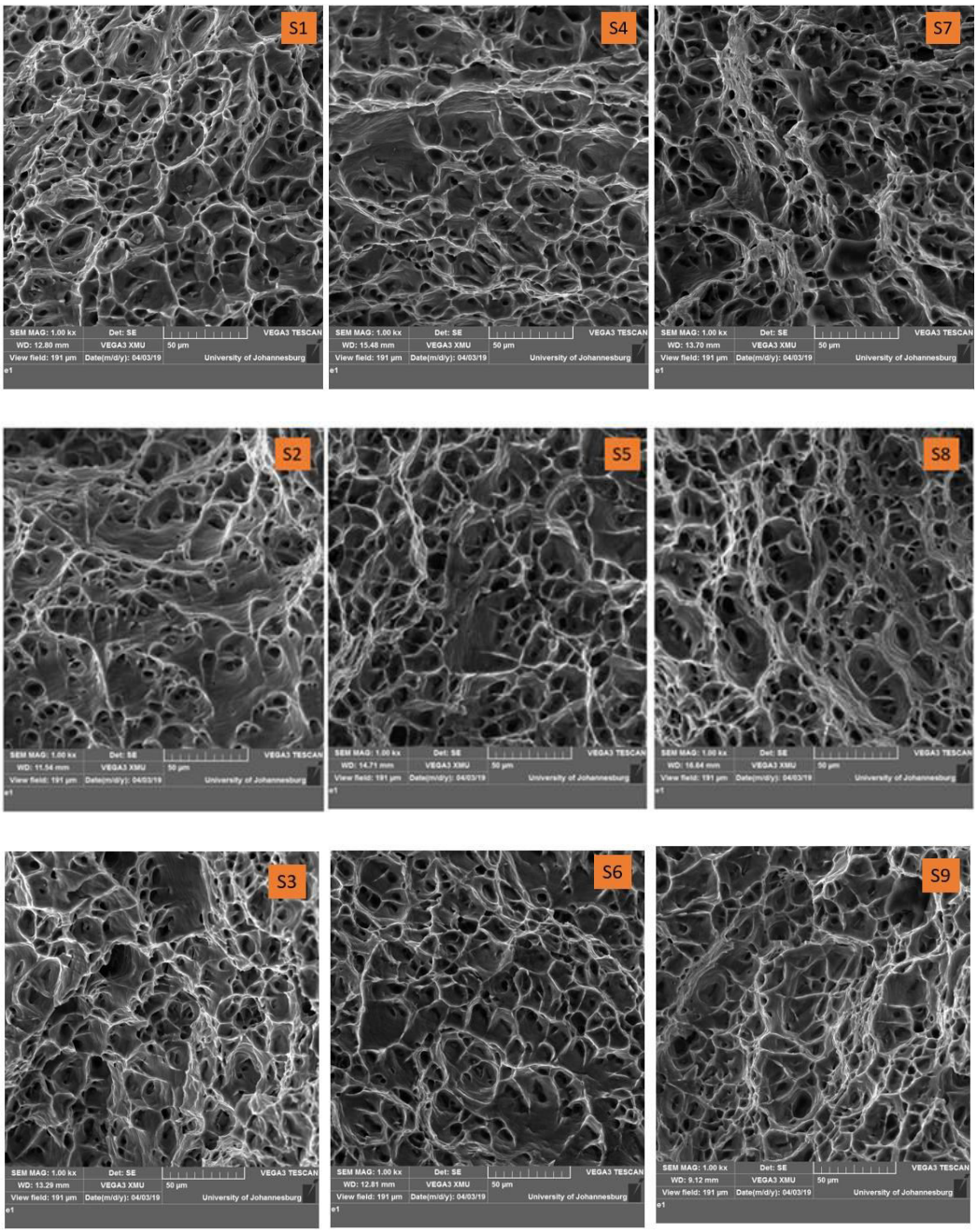

Figure-8. SEM image of the fracture surfaces of the produced spot welds samples.

CONCLUSIONS

This research includes thorough research on characterizing friction stir spot welding of aluminium alloys AA5058-H116 and a critical review of the literature. The purpose of this study was to friction stir spot weld two identical aluminium alloy lap-sheets and assess the changing properties, including tensile characteristics, macrographic, and fractographic investigations. The welded samples were subjected to mechanical tests to meet the goals and objectives of the study. The newly manufactured aluminium metal matrix using friction stir spot welding was found to have outstanding mechanical and metallurgical qualities. It could be employed in severe environments, particularly in the marine, aerospace, automotive, and construction industries. From the experimental reports, results, and discussion, the following findings can be inferred:

a) It was established that the values of the tensile shear strength (TSS) and tensile yield strength (TYS), and the fracture force (F.F.) were determined for the welded samples during the tensile test. The F.F. was recorded at 900 rpm at 5 sec, 10 sec, and 15 seconds, corresponding to 12.65, 13.02, and 13.17 kN, respectively, which produced tensile shear strength, TSS of 351.62 MPa, 361.70 MPa as well as 365.84 MPa, respectively. At this point, their tensile yield strength (TYS) generated 274.70 MPa, 266.86 MPa,

and 273.93 MPa with corresponding elongations of 11.18 %, 12.61 %, and 16.67 %, and these were the highest values produced during the spot welds. The TSS produced at 900 rpm are all higher than the UTS of the B.M., which is 351.62 MPa, 361.70 MPa and 365.84 MPa as against 317 MPa of the B.M., and this may be attributed to the efficacy of the effective and homogenous stirring of the zones at that parameters.

b) The maximum fracture force and tensile shear strength occurred at a rotational speed of 900 rpm for all dwell time, while the least values occurred at 600 rpm.

c) The fractography of the fracture surfaces from a tensile test revealed that all the fracture surfaces show ductility behaviours through the morphological examination of the rupture surfaces. This ductility pattern of the fracture surfaces was due to considerable and significant plastic deformation, which was caused enormous load. The ductile fracture is a kind of rupture that is accompanied by severe plastic deformation or "necking", generally just before an actual fracture occurs.

REFERENCES

[1] M. P. Mubiayi and E. T. Akinlabi. 2015. An overview Onfriction stir spot welding of dissimilar materials. Transactions on Engineering Technologies. pp. 537-549.

[2] O. M. Ikumapayi and E. T. Akinlabi. 2019. Recent advances in keyhole defects repairs via refilling friction stir spot welding. Materials Today: Proceedings. 18: 2201-2208.

[3] M. Li, C. Zhang, D. Wang, L. Zhou, D. Wellmann and Y. Tian. 2020. Friction stir spot welding of aluminum and copper: A review. Materials. 13: 156.

[4] N. Sridharan, D. Isheim, D. N. Seidman and S. S. Babu. 2017. Colossal super saturation of oxygen at the iron-aluminum interfaces fabricated using solid state welding. Scr. Mater. 130: 196-199.

[5] A. Nassiri, T. Abke and G. Daehn. 2019. Investigation of melting phenomena in solid-state welding processes. Scr. Mater. 168: 61-66.

[6] O. Masaki, T. Yuichiro, M. Katashi, Y. Toshiaki and F. Masahiro. 2015. Fatigue behaviour of aluminium alloy/steel joints by spot friction stirring. Welding International. 29: 96-102.

[7] A. Gerlich, P. Su and T. North. 2005. Tool penetration during friction stir spot welding of Al and Mg alloys. J. Mater. Sci. 40: 6473-6481.

[8] Z. Shen, Y. Ding and A. P. Gerlich. 2020. Advances in friction stir spot welding. Critical Reviews in Solid State and Materials Sciences. 45: 457-534.

[9] N. D. Alexopoulos, A. A. Gialos, V. Zeimpekis, Z. Velonaki, N. Kashaev, S. Riekehr and A. Karanika. 2016. Laser beam welded structures for a regional aircraft: weight, cost and carbon footprint savings. J. Manuf. Syst. 39: 38-52.

[10] A. Kumar, R. Singh and I. Singh. 2017. A review of metal inert gas welding on aluminium alloys. International Journal of Engineering Sciences & Research Technology. 6: 453-456.

[11] N. E. Prasad and R. J. Wanhill. 2017. Aerospace Materials and Material Technologies. Springer.

[12] R. Tamasgavabari, A. R. Ebrahimi, S. M. Abbasi and A. R. Yazdipour. 2018. The effect of harmonic vibration with a frequency below the resonant range on the mechanical properties of AA-5083-H321 aluminum alloy GMAW welded parts. Materials Science and Engineering: A. 736: 248-257.

[13] C. Zhu, J. Cheon, X. Tang, S. Na and H. Cui. 2018. Molten pool behaviors and their influences on welding defects in narrow gap GMAW of 5083 Al-alloy. Int. J. Heat Mass Transfer. 126: 1206-1221.

[14] O. O. Abegunde, E. T. Akinlabi and D. Madyira. 2017. Microstructural Evolution and Mechanical Characterizations of AL-TiC Matrix Composites Produced via Friction Stir Welding. Materiali in Tehnologije. 51: 297-306.

[15] O. O. Abegunde, E. T. Akinlabi and D. M. Madyira. 2015. Microstructural characterization of friction stir lap welds of aluminium incorporated with titanium carbide.

[16] Y. Su, X. Hua and Y. Wu. 2013. Effect of input current modes on intermetallic layer and mechanical property of aluminum-steel lap joint obtained by gas metal arc welding. Materials Science and Engineering: A. 578: 340-345.

[17] R. Qiu, H. Shi, K. Zhang, Y. Tu, C. Iwamoto and S. Satonaka. 2010. Interfacial characterization of joint between mild steel and aluminum alloy welded by resistance spot welding. Mater Charact. 61: 684-688.

[18] Y. Zhang, Y. Li, Z. Luo, T. Yuan, J. Bi, Z. M. Wang, Z. P. Wang and Y. J. Chao. 2016. Feasibility study of

dissimilar joining of aluminum alloy 5052 to pure copper via thermo-compensated resistance spot welding. Mater Des. 106: 235-246.

[19] P. Mastanaiah, A. Sharma and G. M. Reddy. 2018. Process parameters-weld bead geometry interactions and their influence on mechanical properties: A case of dissimilar aluminium alloy electron beam welds. Defence Technology. 14: 137-150.

[20] ASTM. 2013. E8 / E8M-13a, Standard Test Methods for Tension Testing of Metallic Materials, ASTM International, West Conshohocken, PA, 2013, www.astm.org.

[21] ASTM. 2021. E8 / E8M-21, Standard Test Methods for Tension Testing of Metallic Materials, ASTM International, West Conshohocken, PA, 2021, www.astm.org.

[22] D. Mulaba-Kapinga, K. D. Nyembwe, O. M. Ikumapayi and E. T. Akinlabi. 2020. Mechanical, electrochemical and structural characteristics of friction stir spot welds of aluminium alloy 6063. Manufacturing Review. 7: 25.

[23] J. K. Paik. 2009. Mechanical properties of friction stir welded aluminum alloys 5083 and 5383. International Journal of Naval Architecture and Ocean Engineering. 1: 39-49.

[24] Z. Ma, A. Feng, D. Chen and J. Shen. 2018. Recent advances in friction stir welding/processing of aluminum alloys: microstructural evolution and mechanical properties. Critical Reviews in Solid State and Materials Sciences. 43: 269-333.

[25] Y. Chen, H. Ding, J. Li, Z. Cai, J. Zhao and W. Yang. 2016. Influence of multi-pass friction stir processing on the microstructure and mechanical properties of Al-5083 alloy. Materials Science and Engineering: A. 650: 281-289.

[26] K. Vasu, H. Chelladurai, A. Ramaswamy, S. Malarvizhi and V. Balasubramanian. 2019. Effect of fusion welding processes on tensile properties of armor grade, high thickness, non-heat treatable aluminium alloy joints. Defence Technology. 15: 353-362.

[27] D. Zhang, Z. Yue, M. Dong, G. Wang, A. Wu, J. Shan, D. Meng, X. Liu, J. Song and Z. Zhang. 2019. Effects of weld penetration on tensile properties of 2219 aluminum alloy TIG-welded joints. Transactions of Nonferrous Metals Society of China. 29: 1161-1168.

[28] G. Wang, L. Quan, Y. Li, A. Wu, D. YAN and H. W.U. 2017. Effects of weld reinforcement on tensile behavior and mechanical properties of 2219-T87 aluminum alloy TIG welded joints. Transactions of Nonferrous Metals Society of China. 27: 10-16.

[29] N. D. Alexopoulos, T. N. Examilioti, V. Stergiou and S. K. Kourkoulis. 2016. Tensile mechanical performance of electron-beam welded joints from aluminum alloy (Al-Mg-Si) 6156. Procedia Structural Integrity. 2: 3539-3545.

[30] H. Peng, D. Chen, X. Bai, X. She, D. Li and X. Jiang. 2019. Ultrasonic spot welding of magnesium-to-aluminum alloys with a copper interlayer: Microstructural evolution and tensile properties. Journal of Manufacturing Processes. 37: 91-100.

[31] F. Mirza, A. Macwan, S. Bhole, D. Chen and X. Chen. 2017. Microstructure, tensile and fatigue properties of ultrasonic spot welded aluminum to galvanized high-strength-low-alloy and low-carbon steel sheets. Materials Science and Engineering: A. 690: 323-336.

[32] Y. Bozkurt, S. Salman and G. Çam. 2013. Effect of welding parameters on lap shear tensile properties of dissimilar friction stir spot welded A.A. 5754-H22/2024-T3 joints. Science and Technology of Welding and Joining. 18: 337-345.

[33] M. Kulekci. 2014. Effects of process parameters on tensile shear strength of friction stir spot welded aluminium alloy (EN AW 5005). Archives of Metallurgy and Materials. Vol. 59.

[34] H. Aydın, A. Bayram, A. Uğuz and K. S. Akay. 2009. Tensile properties of friction stir welded joints of 2024 aluminum alloys in different heat-treated-state. Mater Des. 30: 2211-2221.

[35] L. Trueba Jr, G. Heredia, D. Rybicki and L. B. Johannes. 2015. Effect of tool shoulder features on defects and tensile properties of friction stir welded aluminum 6061-T6. J. Mater. Process. Technol. 219: 271-277.

[36] P. Kucharczyk, M. Madia, U. Zerbst, B. Schork, P. Gerwien and S. Münstermann. 2018. Fracture-mechanics based prediction of the fatigue strength of

weldments. Material aspects. Eng. Fract. Mech. 198: 79-102.

[37] Y. Guo and F. Wang. 2019. Dynamic fracture properties of 2024-T3 and 7075-T6 aluminum friction stir welded joints with different welding parameters. Theor. Appl. Fract. Mech. 104: 102372.

[38] C. Jonckheere, B. de Meester, C. Cassiers, M. Delhaye and A. Simar. 2012. Fracture and mechanical properties of friction stir spot welds in 6063-T6 aluminum alloy. The International Journal of Advanced Manufacturing Technology. 62: 569-575.

[39] O. Ikumapayi, E. Akinlabi, A. Sharma, V. Sharma and O. Oladijo. 2020. Tribological, structural and mechanical characteristics of friction stir processed aluminium-based matrix composites reinforced with stainless steel micro-particles. Engineering Solid Mechanics. 8: 253-270.